minerals

MDPI

Article

The Study of Olivine Inclusions in Diamonds from Liaoning, China and the Evaluation of Related Thermometers

Linli Qin [1], Guanghai Shi [2,*], Xin Zhao [1] and Zhenyu Chen [3]

[1] School of Gemology, China University of Geosciences (Beijing), Beijing 100083, China; 3009200005@email.cugb.edu.cn (L.Q.); zhaoxin@cugb.edu.cn (X.Z.)
[2] State Key Laboratory of Geological Processes and Mineral Resources, China University of Geosciences (Beijing), Beijing 100083, China
[3] Key Laboratory of Metallogeny and Mineral Assessment, Ministry of Natural Resources, Institute of Mineral Resources, Chinese Academy of Geological Sciences, Beijing 100037, China; czy7803@163.com
* Correspondence: shigh@cugb.edu.cn; Tel.: +86-010-8232-2107

Abstract: Olivine is the most abundant mineral in mantle peridotite and a typical inclusion in diamonds, providing essential evidence for the characterization of the diamondiferous lithospheric mantle. Three olivine inclusions in diamonds (Ol_{Dia}) from Liaoning in the North China Craton (NCC) were exposed for in situ measurements, and the compositional data of 62 other Ol_{Dia} from Liaoning were collected based on previous reports. The enrichment of TiO_2 (>0.1 wt.%) with high Cr# (>50; Cr# = 100Cr/(Cr + Al) by atom) was revealed, despite the predominance of depleted TiO_2 contents and high Mg# (92.8–93.2; Mg# =100Mg/(Mg + Fe) by atom) for Ol_{Dia}. Silica fluid accompanying olivine still trapped in the host diamond was recognized using Raman spectroscopy. Three thermometers were applied to the Ol_{Dia}, based on the data from Laser Ablation Inductively Coupled Plasma Mass Spectrometry (LA-ICP-MS) and Electron Probe Micro-Analysis (EPMA), and a temperature range (T^{LA} and T^{EPMA}) of 1080–1380 °C was yielded. With respect to the T^{LA}, Al-in-olivine thermometers were preferred, although there was a smaller deviation between T^{EPMA} and T^{LA} when using the Cr-in-olivine thermometer. The results of these thermometers show a high correlation with T^{EPMA}, enabling their application based on EPMA data. Projections onto 39–42 mW/m^2 model geotherms underline a diamondiferous base of the lithospheric mantle beneath the NCC. The lithospheric mantle is characterized by refractory and depleted sections, where enrichment metasomatism may have occurred at the lower roots (161–178 km).

Keywords: diamond; olivine inclusion; thermometer; Liaoning; lithospheric mantle; North China Craton

Citation: Qin, L.; Shi, G.; Zhao, X.; Chen, Z. The Study of Olivine Inclusions in Diamonds from Liaoning, China and the Evaluation of Related Thermometers. *Minerals* **2024**, *14*, 850. https://doi.org/10.3390/min14090850

Academic Editor: Jordi Ibanez-Insa

Received: 23 June 2024
Revised: 20 August 2024
Accepted: 21 August 2024
Published: 23 August 2024

1. Introduction

Diamonds are renowned in various professions for their remarkable physical attributes and chemical properties. As a mantle-derived mineral, diamonds protect their mineral inclusions from subsequent modification by kimberlite magma, providing original samples of the deep Earth [1]. Wafangdian in Liaoning Province is one of the most important localities for diamonds in China, with more than 120 diamond-related rock bodies having been discovered [2,3]. Liaoning diamonds commonly contain olivine as a primary inclusion [4–8], which is typical of peridotitic paragenesis [9]. Olivine is one of the most important rock-forming minerals in mantle peridotite; therefore, obtaining the geochemical characteristics of olivine included in diamonds is significant for tracing the geological processes of the underlying lithospheric mantle.

Olivine represents a continuous solid solution between two endmembers, namely forsterite (Mg_2SiO_4, Fo = 100) and fayalite (Fe_2SiO_4, Fa = 100). The composition of olivine in mantle rocks remains relatively consistent compared to those of other rock-forming minerals like garnet, spinel, orthopyroxene and clinopyroxene, with almost all mantle olivines falling in the range of Fo~89–94 [10]. The forsterite content and the Mg# (100Mg/(Mg + Fe)

by atom) are also considered as crucial indicators for the degrees of depletion for the lithospheric mantle [11,12]. In addition, trace elements like Ti are strongly incompatible within olivine and other rock-forming minerals in the Earth's mantle, closely correlating with the overall content of the related rocks [10,13]. With the development of high-precision analysis techniques such as Laser Ablation Inductively Coupled Plasma Mass Spectrometry (LA-ICP-MS), Secondary Ion Mass Spectrometry (SIMS) and Electron Probe Micro-Analysis (EMPA) in minerals, trace elements in olivine have become a new research topic in recent years to trace the petrogenesis of related rocks and geological events, such as the partial melting of the mantle, mantle metasomatism, and the early crystallization of magma [14].

The concentration of some trace elements in olivine, such as Cr, Al, V, Sc, Ca, Na, etc., are mainly influenced by the equilibrium temperature of the host rock [10,15–18]. This characteristic enables the employment of certain elements in olivine as a simple geothermometer, including the Al-in-olivine thermometer of garnet peridotite [10,19] and the Cr-in-olivine thermometer [18]. For olivine in mantle peridotite, the first Al-in-Olivine thermometer was calibrated on mantle xenoliths by [10]. This thermometer is applicable for olivine inclusions in diamonds. De Hoog also provided a Cr-in-olivine thermometer as an alternative when the Al content in olivine cannot be accurately measured. Although the Al- and Cr- thermometers have been widely applied in the study of mantle peridotitic olivine, the field of diamond inclusions remains relatively unexplored [15,19,20].

Here, we report the discovery of single olivine inclusions and one touching pair of olivines with a garnet within Liaoning diamonds in China. We present in situ data on the olivine inclusions in three diamonds and 62 other olivine inclusions in Liaoning diamonds from previous studies [4–8], and we discuss the source conditions and evaluated temperature of the lithospheric mantle where diamonds precipitate using three olivine thermometers. Our study also provides intrinsic information for understanding ancient mantle in the North China Craton (NCC).

2. Materials and Methods

In this study, we have selected four diamond crystals (Figure 1) containing olivine inclusions among a total of 111 samples from Wafangdian, Liaoning Province, China. Diamond L1-2 contains one olivine grain touching a garnet, while the others contain isolated olivine grains. These diamond samples were polished along the crystals' surface to expose the olivine inclusions. However, the deep-located olivine inclusion in L1-14 has failed to be exposed to the polished surface because further exhumation may lead to the destruction of other inclusions. Next, in situ tests were conducted directly on the exposed plane of the inclusions.

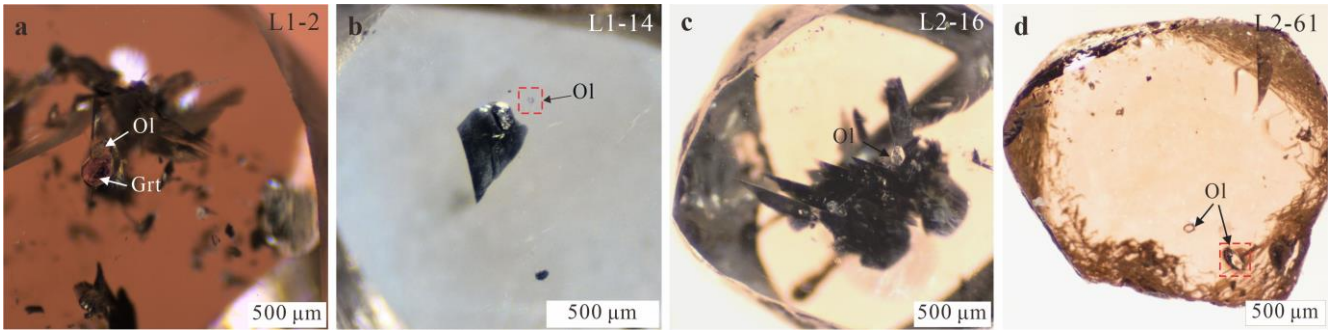

Figure 1. Olivine inclusions in diamond crystals from Liaoning. (**a**) Touching olivine-garnet pair in diamond L1-2. (**b**) Single olivine crystal in diamond L1-14, highlighted in red box. (**c**) Single olivine crystal in diamond L2-16. (**d**) Multiple transparent inclusions, with two confirmed as olivine; the larger inclusion, highlighted by a red box, has been exposed for in situ analysis.

Raman. Basic phases were confirmed using an HR-Evolution Raman spectrometer at the School of Gemology, China University of Geosciences, Beijing (CUGB). The tests were

conducted with an excitation wavelength of 532 nm, a testing power ranging from 50 to 100 mW, a scanning wavenumber range ranging from 50 to 4000 cm^{-1}, and a data acquisition time of 3 s; acquisition was performed twice and tested under liquid nitrogen temperature conditions.

EPMA. The composition of the inclusions was determined at the MNR Key Laboratory of Metallogeny and Mineral Assessment, Institute of Mineral Resources, Chinese Academy of Geological Sciences, with a JXA-8230 Electron Probe Micro-Analyzer (JEOL, Tokyo, Japan) equipped with four wavelength-dispersive spectrometers. Before analysis, the samples were coated with 20 nm thin conductive carbon film. During the tests, an accelerating voltage of 15 kV, a beam current of 20 nA and a 1–5 μm spot size were used. Counting times range from 10 to 20 s for major elements. For trace elements (including Al and Cr in olivine), the counting times were set to 50–100 s to improve precision. The standards used in our EPMA laboratory are as follows: Jadeite/Quartz is used as a standard for Si, Forsterite for Mg, Almandine for Al, Topaz for F, Synthetic Potassium Niobate for K, Wollastonite for Ca, Magnetite for Fe, Rutile for Ti, Apatite for P, Cr_2O_3 for Cr, MnO for Mn, NiO for Ni, Synthetic Calcium Vanadate for V and NaCl for Cl. Limit of detection (LOD) for the elements are as follows: Si: 83–96 ppm, Mg: 65–74 ppm, Al: 77–81 ppm, F: 1098–1174 ppm, K: 48–53 ppm, Ca: 64–77 ppm, Fe: 87–99 ppm, Ti: 236–244 ppm, P: 84–93 ppm, Cr: 112–137 ppm, Mn: 104–113 ppm, Ni: 136–154 ppm, V: 104–192 ppm and Cl: 222–289 ppm. The data were corrected online using a modified ZAF (atomic number, absorption and fluorescence) correction procedure.

According to global studies of mantle olivine xenoliths, the Al content in olivine generally ranges from 30 to 120 ppm. Notably, olivine inclusions in diamonds show even higher Al potential; an example is the Al~50–290 ppm in olivine inclusions within Cullinan diamonds [20]. For Cr in olivine inclusions, although there is a lack of related datasets with LA-ICP-MS or SIMS methods, EPMA data indicate that Cr in olivine inclusions within peridotitic diamonds ranges from 0 to 1.36 wt.%, with a median of 0.06 wt.% [12]. Although the EPMA LODs for Al and Cr reported above are relatively high, we believe our data to be reliable and accurate due to the increased counting times during measurements.

LA-ICP-MS. To ensure data accuracy, Laser Ablation Inductively Coupled Plasma Mass Spectrometry was used for testing. Since most inclusions are relatively small (shortest dimension 50–100 μm), and the pre-polishing process can make them even thinner, it is important to choose a smaller ablation spot size. The ablation process should be conducted on the thicker area of the inclusion, which should be closely monitored to avoid penetration of the inclusion. LA-ICP-MS was conducted at the in situ Minerals Lab, School of Resources and Environmental Engineering, Hefei University of Technology, using an IRIDIA Laser Ablation System coupled with an Agilent 7900 ICP-MS. For spot analysis, a 25–30 μm spot size was applied with an energy density of ~2–4 J/cm^2 and a repetition rate of 7 Hz. Each analysis contained 20 s for measuring the gas blank and 40 s for laser ablation. Different silicate glass reference materials, including NIST610, GSC-1G, GSD-1G and BCR-2G were used as external standards. The recommended values of the elements in the standard glasses are taken from the GeoReM database (http://georem.mpch-mainz.gwdg.de/, accessed on 2 June 2024). The data processing was performed using the SpotAnalysis V4. LOD for certain elements in olivine: Al: 1.7–3.1 ppm, Ti: 14–24 ppm, Cr: 9.1–16 ppm.

Meanwhile, compositional information of the other 62 olivine grains in the Liaoning diamonds was also collected from previous reports [4–8]. The dataset is restricted due to the scarcity of reports on the specific composition of olivine inclusions from Liaoning [4–8]. Out of them, 35 were further selected for temperature estimation, which were tested by the in situ method after polishing the host diamond. Their composition included $Al_2O_3 > 0$ wt.%, $Cr_2O_3 > 0$ wt.%, Total~98.5–101.5 wt.% (details in Supplementary Material). The exclusion of certain data is necessary because some studies expose the inclusion by burning or cracking the host diamond for compositional analysis. These methods lead to the environmental change of olivine inclusions, resulting in changes in Fe^{3+} content, residual stress and others. Such changes could significantly impact temperature estimation.

In any case, the exclusion of low Al and Cr results from the comparison of different Al- and Cr- in olivine thermometers. Despite there being differences in the testing conditions and equipment, the data still clarify the formation conditions of Liaoning diamonds.

3. Results

While diamond L2-16 exhibits as an irregular plate, the remaining samples all display octahedral shapes. When observed under a microscope, olivine inclusions appear as colorless euhedral grains with excellent transparency, ranging in size approximately from 20 μm × 20 μm to 100 μm × 50 μm. The Raman spectra show sharp peaks at 824 and 855 cm^{-1} for all the investigated olivine inclusions in the diamonds (Ol_{Dia}) (Figure 2), showing relatively strong Raman scattering intensity and a narrow full width at half maximum (FWHM). Notice there are two peaks with relatively wide FWHM at 679 cm^{-1} and 780 cm^{-1} in L1-14, indicative of a non-crystalline phase. Previous studies identified the two wide peaks (617–671 cm^{-1} and 761–825 cm^{-1}) around different mineral inclusions within the diamond in Raman spectra [21–23], and attributed these peaks to $Si_2O(OH)_6$ dimers and $Si(OH)_4$ monomers in the aqueous fluid, respectively. Therefore, it is believed that these two similar peaks in L1-14 represent the presence of silica fluid.

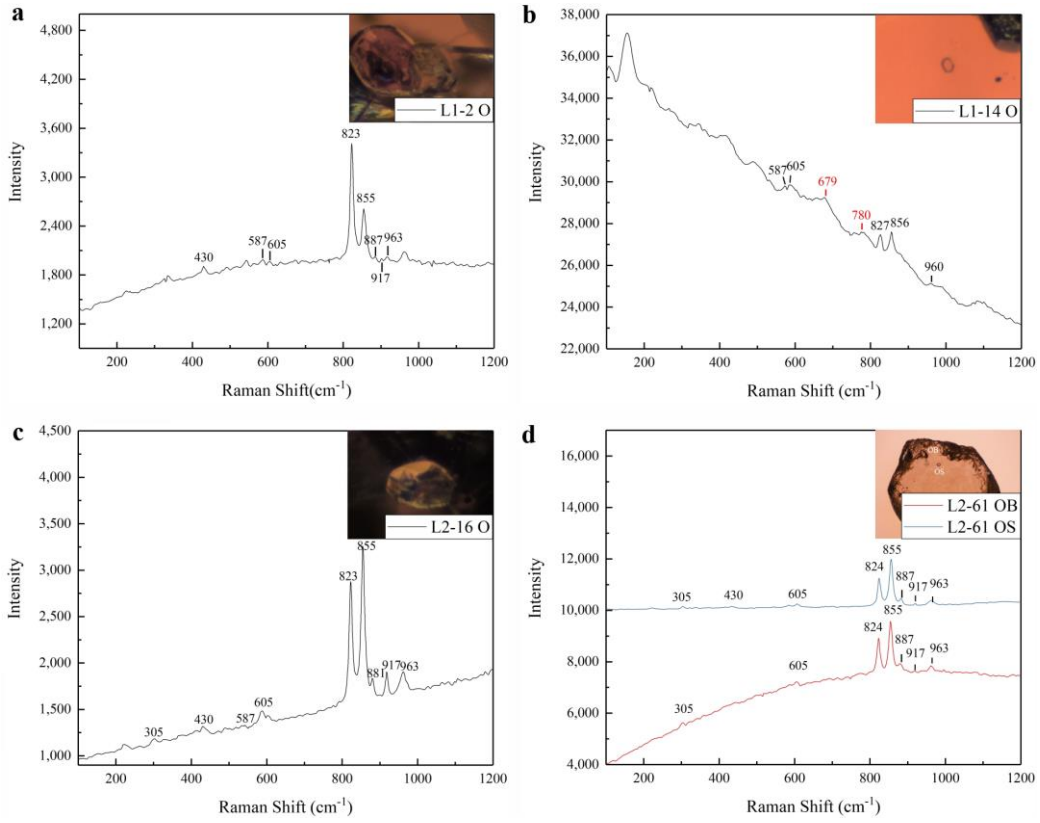

Figure 2. Raman spectra of olivine inclusions in diamonds (Ol_{Dia}) from Liaoning. All Ol_{Dia} show sharp peaks at around 824 and 855 cm^{-1}. Unexposed olivine inclusions (**b**,**d**) have weaker signals compared to exposed ones (**a**,**c**). Additionally, L2-61 contains small, colorless, transparent inclusions that cannot be identified by Raman spectroscopy due to their greater depth in the host diamond. (**b**) includes two wide peaks at 679 cm^{-1} and 780 cm^{-1}, with the full width at half maximum more than five times wider than those of the olivine crystal, indicating a non-crystalline phase.

The olivine inclusion compositions in L1-2, L2-16 and L2-61 were determined using EPMA and LA-ICP-MS (Table 1), and the EPMA results of 62 other grains of Ol_{Dia} from Liaoning were collected [4–6]. This enabled us to conduct in-depth comparisons with those of the previous studies and analyze our research findings. Despite the differences

in testing conditions and equipment, the data still clarify the formation conditions of Liaoning diamonds.

Table 1. Compositional data of olivine and coexisting garnet inclusions in investigated diamonds from Liaoning obtained using EPMA and LA-ICP-MS.

		L1-2-O2	L2-16-O3	L2-61-O2	L1-2-G-3	L1-2-g-1
EPMA (wt.%)	SiO_2	39.70	41.57	42.47	41.38	40.85
	TiO_2	0.04	0.00	0.00	0.00	0.04
	Al_2O_3	0.01	0.03	0.01	18.53	20.69
	Cr_2O_3	0.08	0.08	0.06	8.10	6.68
	FeO	7.17	6.62	6.68	6.21	7.13
	MnO	0.11	0.07	0.15	0.28	0.21
	MgO	52.78	50.79	50.13	22.18	20.60
	NiO	0.31	0.27	0.29	0.00	0.03
	CaO	0.03	0.02	0.05	3.27	3.23
	Na_2O	0.02	0.00	0.02	0.00	0.20
	K_2O	0.01	0.00	0.00	0.06	0.37
	Total	100.26	99.45	99.86	100.01	100.03
	Si	0.96	1.01	1.02	2.96	2.93
	Ti	0.00	0.00	0.00	0.00	0.00
	Al	0.00	0.00	0.00	1.56	1.75
	Cr	0.00	0.00	0.00	0.46	0.38
	Fe^{3+}				0.06	0.08
	Fe^{2+}	0.15	0.13	0.13	0.32	0.35
	Mn	0.00	0.00	0.00	0.02	0.01
	Mg	1.91	1.84	1.80	2.37	2.20
	Ni	0.01	0.01	0.01	0.00	0.00
	Ca	0.00	0.00	0.00	0.25	0.25
	Na	0.00	0.00	0.00	0.00	0.03
	K	0.00	0.00	0.00	0.01	0.03
	Total	3.03	2.99	2.98	8.00	8.00
	Fo	92.82	93.12	92.90		
	Mg#	92.92	93.19	93.04	86.42	83.7
	Cr#	84.29	69.01	87.39		
	Ca/Al	2.73	0.73	7.58		
	Ti	n.d.	n.d.	n.d.		
LA-ICP-MS (ppm)	Al	72.3	66.5	52.8		
	Cr	268	571	422		

The olivine in diamond L1-2 coexists with a touching garnet. EPMA data were primarily obtained from a polished, smooth surface of the inclusion, with the table showing data from the core area. The formulae for olivine and garnet were calculated on the basis of four oxygens. LA-ICP-MS was conducted at the core area of the inclusion. "n.d." refers to "not detected".

The olivine inclusions in the Liaoning diamonds from this study and previous research also show Al_2O_3 and Cr_2O_3 as temperature-sensitive elements. The LA-ICP-MS result shows the content of Al varied between 52.8 and 72.3 ppm, and Cr between 816 and 846 ppm in our study. Due to the lack of LA-ICP-MS or SIMS data available for Ol_{Dia} in Liaoning, we can only rely on the EPMA data for a rough comparison. Based on the data collected from the 62 Ol_{Dia}, the content of Al_2O_3 varied between 0.00 and 0.34 wt.%, with a median of 0.02, while the content of Cr_2O_3 varied at a relatively narrow range (0.01–0.13 wt.%), with a median of 0.06 wt.%. Almost 92% of the 65 samples have less than 0.1 wt.% Cr_2O_3, corresponding to the typical Cr_2O_3 content found in Ol_{Dia} around the world [12]. In contrast, the olivines included in garnet peridotite xenoliths show less Cr_2O_3 (the mean is 0.03 ± 0.02 wt%) [12].

When we created a scatter plot of Cr#(100Cr/(Cr + Al) by atom) and TiO_2 (Figure 3), some points of Ol_{Dia} from Liaoning fell on the horizontal axis (*X*-axis), indicating an extremely low Ti content, which could be possibly influenced by the limitations or errors of the testing technique. Even though these points may not accurately reflect the actual

Ti-content, the results still reflect the extremely low Ti in some Ol_{Dia}. While our sample shows a Cr# range from 69.0 to 87.4, the data in the previous studies on Liaoning diamonds show a wider range (8.98~100.00). Notably, one sample shows the content of Cr# is below 20, while the other nine samples have a Cr# value of 100. The Ol_{Dia} in this study has a TiO_2 range from 0 to 0.04 wt.% detected using EPMA. There is slightly more TiO_2 (0–0.02 wt.%) in the previously studied Liaoning diamonds, among which 61% were below the LOD of EPMA.

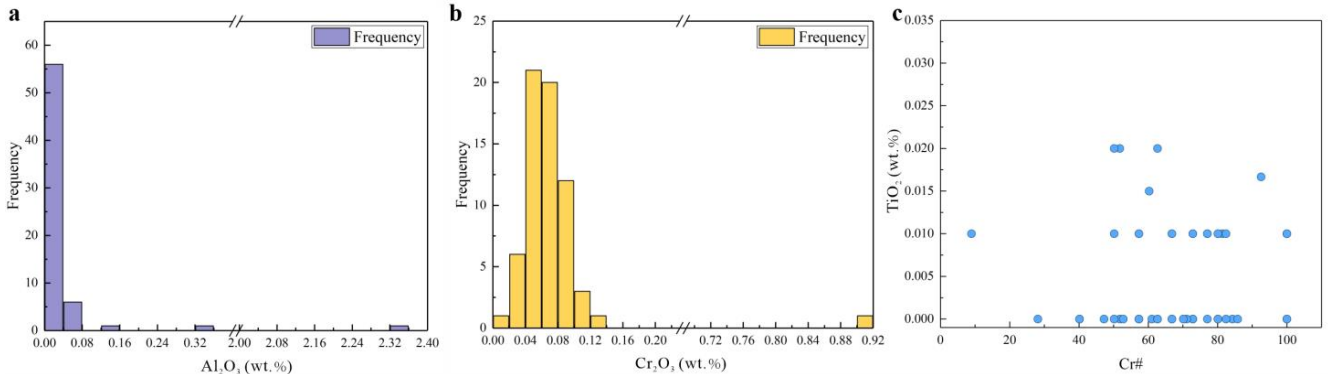

Figure 3. Elemental composition analysis diagram of 65 olivine inclusions from Liaoning diamonds; data were collected from this study and previous studies [4–8]. (**a**,**b**) include histograms of Al_2O_3 and Cr_2O_3. (**c**) includes a scatter plot of Cr# and TiO_2.

The results revealed a high content of forsterite with a range of Fo~92.6–93.1 in our Ol_{Dia}, and the Mg# number was also relatively consistent (92.8–93.2), with a median of 93.1 (Figure 3). This falls within the most two frequently observed ranges of the data from the previous reports on Liaoning Ol_{Dia} (92.5–93.0 and 93.0–93.5), with a median of 92.8; meanwhile, the Mg# of olivines in diamonds worldwide varies with different parageneses (Figure 4). For worldwide Ol_{Dia}, the median Mg# belonging to harzburgitic paragenesis is 93.1, with the highest frequency being between 91.5 and 92, while the median of Mg# number is slightly lower (91.8) for those belonging to lherzolitic paragenesis, with the highest frequency being between 93 and 93.5 [12]. All the investigated Ol_{Dia} belong to peridotitic paragenesis [9].

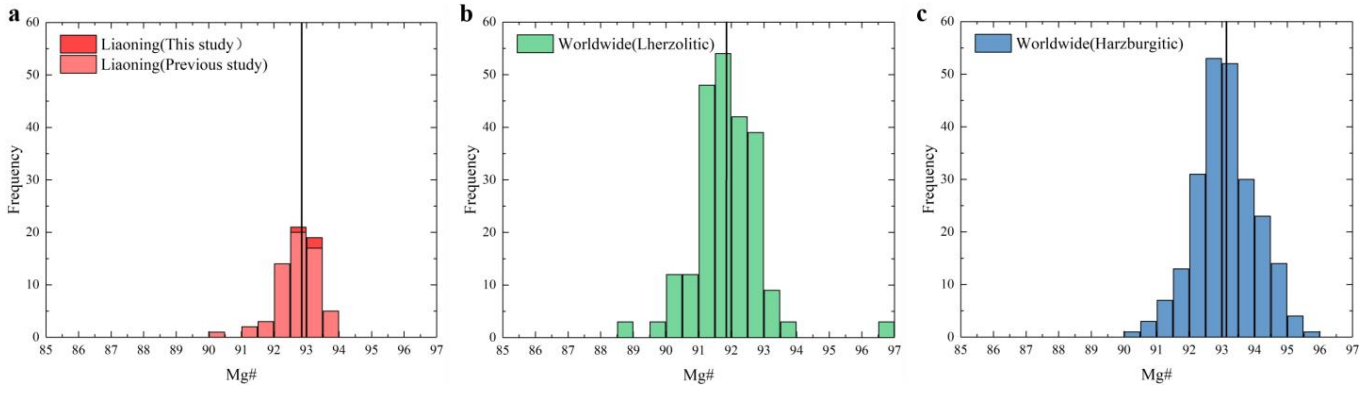

Figure 4. Histograms of molar Mg# of olivine inclusions within diamonds (Ol_{Dia}). (**a**) includes data for Ol_{Dia} from Liaoning, both from this study and previous studies [4–8]; (**b**,**c**) are modified according to [12] for Ol_{Dia} from worldwide belonging to harzburgitic and lherzolitic parageneses.

4. Discussion

The Ol_{Dia} allow for the preservation of original samples from the old mantle, providing evidence of the source conditions and mantle evolution of diamond formation. The Al and Cr are primarily governed by the equilibrium temperature of the host rocks, establishing a

foundation for using olivine inclusions to understand the temperature characteristics of diamond source regions.

4.1. Implications for Refractory Mantle

As a common inclusion in diamonds, olivine is a useful component for understanding mineral paragenesis within the lithospheric mantle beneath the NCC, where most Liaoning diamonds derive. The olivine inclusions in diamonds (Ol_{Dia}) belong to a peridotitic suite, which is subdivided into lherzolitic, harzburgitic and wehrlitic parageneses [9]. It should be noted that both harzgurgitic and lherzolitic peridotites are the main source rocks for diamond formation within the mantle, and harzburgite contains most cratonic diamonds [24]. The specific subdivision of olivine has traditionally depended on its coexisting garnet or pyroxene inclusions. Based on the Cr_2O_3-CaO diagrams of the coexisting garnet in L1-2 (Figure 5), its olivine inclusion is subdivided into a harzburgitic suite [9,12]. Unfortunately, most Ol_{Dia} from Liaoning are observed without coexisting minerals, preventing the subdivision of mineral paragenesis, which aligns with global research on Ol_{Dia} [12]. Globally, only about 16% of Ol_{Dia} are confirmed to be harzburgitic, and 5% to be lherzolitic.

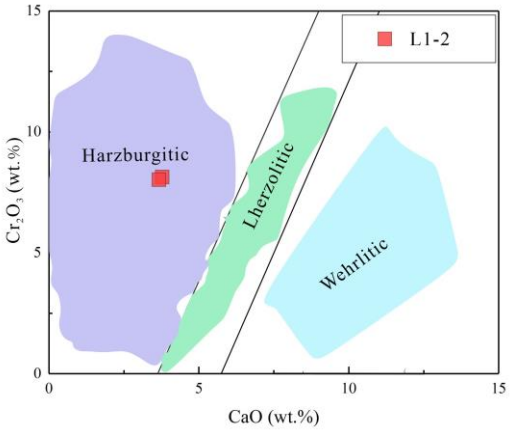

Figure 5. Discrimination diagrams of different types of diamond based on Cr_2O_3–CaO (wt%) for peridotitic garnet inclusions in diamonds. Fields for different parageneses (harzburgitic, lherzolitic and wehrlitic) are cut off by black lines. Plot of garnet inclusion (two generation) in L1-2 shows harzburgitic paragenesis. Modified after [12].

The Fo value in the olivine and the Mg# are commonly used to evaluate the degree of depletion of the lithospheric mantle [11,12]. The primitive mantle is presumed to be relatively uniform and undifferentiated, with an Mg# number range from 87.4 to 89.3, while the depleted mantle has experienced partial melting processes, with an increase in Mg# in the remaining mantle. In our study, the Mg# content of Ol_{Dia} lies between 92.8 and 93.2, which is consistent with that for olivine xenolith in the kimberlite from Liaoning [25,26] and suggests a similar depletion history in the lithospheric mantle where Liaoning diamonds form. In contrast, the olivine in Cenozoic basalt lherzolite shows a lower Mg# content (<90) in these areas [26]. This demonstrates the transformation of the underlying lithospheric mantle from old, refractory to young, fertile mantle states, which is consistent with the destruction of the NCC [27–30]. In addition, according to the dataset for worldwide Ol_{Dia} by [12], it shows a similar range with olivine xenolith in garnet peridotite in Mg# (median, 91.8; mean, 91.7 $\pm$ 1.3). This range is slightly lower than the results for the investigated samples and the data collected for Liaoning Ol_{Dia}, possibly suggesting a more refractory component for mantle peridotite in the NCC than those from other cratons.

Another noteworthy factor is the influence of Ti and Cr#, which are also used to estimate the degree of melt extraction from the mantle residue [10,16–18]. The content of TiO_2 in olivine is strongly related to the bulk rock concentrations, which are supposed to range from ca. 100 ppm in fertile MORB mantle to below 5 ppm in depleted mantle, with

25% melting and exhaustion of clinopyroxene from the residue [10]. The TiO_2 is expected to show a good correlation with Cr# but is rather poor in this study. Our investigation of the three samples shows Ti as extremely depleted (below LOD of LA-ICP-MS) and Cr# ranges from 65.8 to 80. For the other 62 Ol_{Dia} in Liaoning from previous reports, more than half of them are also depleted in TiO_2 (below LOD of EPMA), and over 90% of the investigated samples show a Cr# number higher than 50. These demonstrate the depletion of mantle peridotites. Notably, the results show 34% of the Liaoning Ol_{Dia} have a relatively rich TiO_2 content ($\geq$0.01 wt.%), suggesting a metasomatism re-fertilization process in the NCC, revealing early melt/fluid activity.

In addition, the observation of such silica fluid provides further evidence for fluid/melt metasomatism. The exact origin of the silica fluid cannot be confirmed based on the existing data. It could be either the primary diamond-forming medium or the typical residue of metasomatic reactions during diamond formation. In any case, it has been argued that silica fluid is closely related to the formation of diamonds. It is generally believed that most diamonds form by metasomatic processes, occurring primarily during the redox–oxidation reactions between C-H-O-N-S dominated fluids/melts and the mantle rocks they penetrate [12,31–34]. The silica fluid has been demonstrated to be common surrounding typical mineral inclusions in diamonds [35]. However, similar reports have not yet been documented in the Liaoning area.

4.2. Temperature Estimation of Liaoning Diamonds Including Olivine

4.2.1. Conventional Thermometers Made of Olivine

As elements Al and Cr in olivine are highly sensitive to temperature, researchers have used the concentration of these elements in olivine as simple geothermometers, including three versions of Al-in-olivine thermometer [10,19,36] and a Cr-in-Olivine thermometer [10]. The Al-in-olivine thermometer proposed by [10] (T [Al-Ol, dH10]) is the most useful for studying garnet peridotitic olivines. It is relatively efficient within the range of 800–1400 °C, with deviation of 15 °C. The expression is as follows:

$$T_{Al-Ol}(^{\circ}\mathrm{C}) = \frac{9423 + 51.4P + 1860Cr\#^{ol}}{\left(13.409 - ln[Al]^{Ol}\right)} - 273 \quad (1)$$

It also requires the Cr in olivines to exist in the form of Cr^{3+}. Previous studies revealed considerable Cr^{2+} in olivine inclusions [10,13,37], excluding T [Al-Ol, dH10] as a reliable thermometer for our Ol_{Dia}. In this situation, [10] proposed a calibrated thermometer (T [Al-Ol, dH10-Dia]):

$$T_{Al-Ol}(^{\circ}\mathrm{C}) = \frac{11959 + 55.6P}{\left(14.530 - ln[Al]^{Ol}\right)} - 273 \quad (2)$$

Despite ignoring Cr#, the calculated average deviation for T is a mere 20 °C. The above thermometers maintain their precision and reliability for olivines in clinopyroxene-free harzburgites and spinel peridotites, with Cr# between 35 and 75. Cr# was also neglected in the calibration by [19], and the expression (T [Al-Ol, Bw17]) is as follows:

$$T_{Al-Ol}(^{\circ}\mathrm{C}) = \frac{11245 + 46.0P}{\left(13.68 - ln[Al]^{Ol}\right)} - 273 \quad (3)$$

This perfectly matches the olivines from cratonic garnet peridotite, with a Cr# number generally greater than 45. The uncertainty of the thermometer is within ±20 °C. To distinguish between olivines from garnet, garnet–spinel and spinel–facies peridotites, [19] also exclude data with a low Al content (<10 ppm). In addition, [19] proposed to project the temperature of the Al-in-olivine thermometer onto the geotherms, and the *P*-*T* could be iteratively calculated to combine Equation (3) with the linear equation of the geotherms [38].

In addition, an alternative Cr-in-olivine thermometer (T [Cr-Ol, dH10]) [10] could be considered when the precise Al content is unavailable and the Cr content is elevated, expressed by

$$T_{Cr-Ol}(^{\circ}\mathrm{C}) = \frac{13444 + 48.5P - 4678Cr\#^{Ol}}{\left(14.53 - ln[Cr]^{Ol}\right)} - 273 \quad (4)$$

The results of the Cr-in-olivine thermometer show an average calculation error within 15 °C for harzburgitic olivine for P within 2.9 kbar, but it is less accurate for garnet–spinel peridotitic olivines. The presence of Cr^{2+} or disequilibrium could also lead to significant deviation.

The olivines included in diamonds are widely believed to represent a garnet peridotitic source, enabling the utilization of these thermometers. The presence of Cr^{2+} in our samples excludes the application of T [Al-Ol, dH10] on our samples. Therefore, we focused on T [Al-Ol, dH10-Dia], T [Al-Ol, Bw17] and T [Cr-Ol, dH10] to evaluate the temperature of Ol_{Dia}.

4.2.2. Temperature Estimation Based on Olivine Inclusions

1. LA-ICP-MS vs. EPMA: Temperature measurements for olivine

Calculations based on three thermometers—T [Al-Ol, dH10-Dia], T [Al-Ol, BW17] and T [Cr-Ol, dH10]—for the two datasets were performed, and the corresponding T^{LA} and T^{EPMA} results are displayed in Table 2. The preset pressure was 52.1 kbar for L1-2, 49.4 kbar for L2-16 and 49.2 kbar for L2-61, according to the in situ X-ray diffraction method [39]. T [Al-Ol, dH10-Dia] only provided valid T estimates for one sample in each dataset, with only one meeting the Cr# requirements (35–75). In contrast, T [Al-Ol, BW17] (with a broader Cr# requirements of >45) successfully estimated T for all three samples. T [Cr-Ol, dH10] was more accurate with harzburgitic olivine but less stable for olivines from garnet–spinel peridotite.

Table 2. Temperature estimation for olivine inclusions in Liaoning diamonds.

	Sample	T [Al-ol, dH10-Dia] (°C)	T [Al-ol, Bw17] (°C)	T [Cr-ol, dH10] (°C)	Average (°C)	Standard Deviation (°C)	Cr#
T^{LA}	L1-2	1176	1178	1169	1175	4	65.8
	L2-16	-	1152	1196	1174	21	81.7
	L2-61	-	1118	1148	1133	14	80.6
T^{EPMA}	L1-2	-	1132	1189	1160	29	84.3
	L2-16	1252	1264	1267	1261	6	64.1
	L2-61	-	1048	1112	1080	32	80.1

T [Al-ol, dH10-Dia] calculations require a Cr# within the range of 35–75, with only one result yielded. The preset pressure used in temperature estimation is L1-2~52.1 kbar, L2-16~49.4 kbar, L2-61~49.2 kbar according to [39]. "T^{LA}" refers to result based on LA-ICP-MS data, while "T^{EPMA}" refers to result based on EPMA data.

LA-ICP-MS data, providing ppm-level precision for Al and Cr concentrations, give far more precise results. An average T^{LA} range of 1133–1175 °C was obtained for the three diamonds based on the LA-ICP-MS data, with the standard deviation (SD) between 4 °C and 21 °C. L1-2 showed the lowest SD (4 °C) among the different thermometers. Note that L1-2 was subdivided into a harzburgitic paragenesis due to the coexisting garnet, which is the optimal paragenesis for T [Cr-Ol, dH10]. In addition, olivine in L2-16 and L2-61 showed higher Cr content than that in L1-2. The higher Cr content suggests a higher amount of Cr^{2+}, which led to increased inaccuracies when using T [Cr-Ol, dH10]. To achieve the best accuracy in Al and Cr data analysis, the use of Al-in-olivine thermometers with the LA-ICP-MS method is recommended.

In contrast, T^{EPMA} data provided an average result ranging from 1080 to 1261 °C, with an SD ranging from 6 to 32 °C. For a certain sample and thermometer, the ΔT ($|T^{LA}$-$T^{EPMA}|$) varied from 15 to 112 °C, with a relatively narrow range of ΔT (20–71 °C) recorded

by T [Cr-Ol, dH10]. It seems that the T^{EPMA} showed fewer inaccuracies with T [Cr-Ol, dH10] than with other thermometers. We speculate that this is due to the higher Cr content in olivine (above LOD of EPMA) than Al content, which allows for more accurate identification using EPMA. Considering the priority of Al-in-olivine thermometers and the systematic errors produced by the Cr-in-olivine thermometer, we propose using the average of T^{EPMA} generated with different thermometers for comparison. This can be supported by the narrower ΔT values obtained from averaging the T^{EPMA} of different thermometers.

2. Temperature Estimation with thermometers based on previous EPMA data

Due to the scarcity of data available for Al and Cr in Ol_{Dia} from Liaoning analyzed using LA-ICP-MS or SIMS, we can only perform temperature evaluations based on their EPMA data. To improve the accuracy of our results, we have re-evaluated the EPMA data from the relevant literature, verifying the testing methods used (an accelerating voltage of 15 kV and a beam current $\geq$10 nA; counting times $\geq$ 15 s; ZAF or PAP correction routine; descriptions of secondary standards). Furthermore, we only included data that were collected in situ by polishing the host diamond, avoiding burning or cracking methods. These methods cause alterations, such as Fe^{2+} oxidation and the elimination of residue strain around inclusions, which may finally lead to inaccuracies in temperature estimation. Moreover, we excluded samples where Al and Cr content was absent, and where Cr# < 35. As a result, only 35 samples were left for temperature estimation.

Next, we employed the thermometers T [Al-Ol, dH10-Dia], T [Al-Ol, BW17] and T [Cr-Ol, dH10] using the PTEXL [40] to constrain the source temperature of the diamonds from Liaoning. The calculation used a preset temperature of 1000 °C and a preset pressure of 50 kbar for all 35 Ol_{Dia} collected. The average 10 kbar adjustment in the preset pressure will lead to a deviation of less than 50 °C in the calculated T for the thermometers. According to the previous studies, most Liaoning diamonds formed at pressures within the range of 50–70 kbar [14]. Therefore, using 50 kbar as the preset pressure may better reflect the actual conditions of most samples.

After calculations using EPMA data for the 35 Ol_{Dia} and sorting each thermometer within the applicable range, a total of 90 T values for temperature were obtained. Estimation based on T [Al-Ol, dH10-Dia] requires Cr# in the range of 35–75; hence, 21 results were yielded for the two thermometers. T [Al-Ol, BW17] provides reliable estimates with Cr# >45, thus yielding 34 results. Finally, T [Cr-Ol, dH10] successfully estimated T for all 35 samples. A scatter plot with error values was drawn for further analysis based on these data (Figure 6). The results showed that the average of the three thermometers ranged from 1114 to 1378 °C, reflecting a relatively stable temperature range of Ol_{Dia} using the three thermometers.

When comparing the results of the different thermometers, we further considered the correlation coefficients and their averages to assess how well each thermometer matched the overall trend. This contributes to understanding the results of the different thermometers and recognizing the potential deviations. Based on an analysis of the correlation matrix (Table 3), it was found that the T values calculated using T [Al-Ol, dH10-Dia] and T [Al-Ol, BW17] were highly consistent, with correlation coefficients close to 1.00. This indicates that the T values calculated using these thermometers were nearly identical. In contrast, T [Cr-Ol, dH10] showed relatively weaker correlations with the other thermometers, especially with T [Al-Ol, BW17], where the correlation was 0.95. This discrepancy could be due to the presence of Cr^{2+} or disequilibrium [10], or the varied inaccuracies with Al and Cr through EPMA, as discussed above. Even though these thermometers may differ in some details and assumptions, the high correlation shows that there is no significant systematic deviation between the calculation results of the different thermometers, indicating that they all provide relatively reliable estimates of the T value of Ol_{Dia}. Furthermore, the high correlation (0.98–1.00) between these thermometers and their average enhances our confidence in the application of the average T. Together with the T^{LA} for the three investigated Ol_{Dia}, we conclude that conditions for diamondiferous lithospheric beneath the NCC include temperatures ranging from 1080 to 1380 °C.

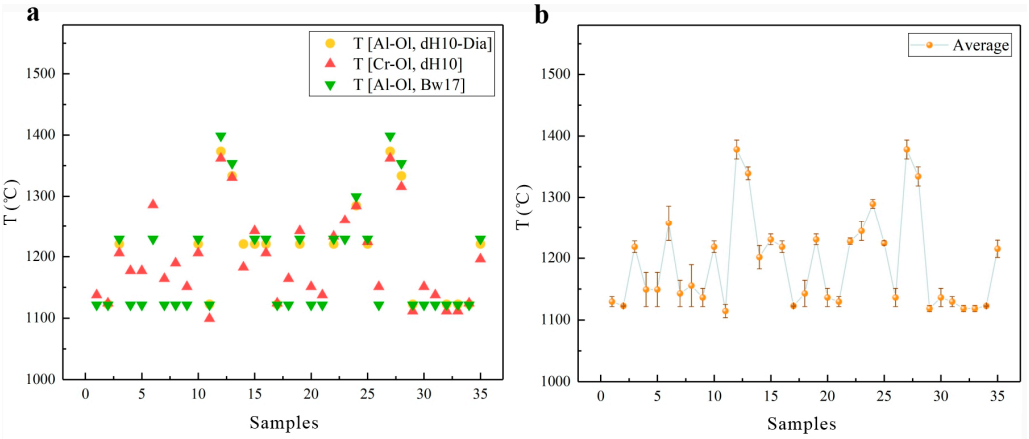

Figure 6. The results of temperature (*T*) estimation of 35 olivines in diamonds (Ol_{Dia}), both from this study and previous studies [4]. The results were calculated using three thermometers (T [Al-Ol, dH10-Dia], T [Cr-Ol, dH10] and T [Al-Ol, BW17]). (**a**) includes a scatter plot of the 90 *T* values calculated based on 35 Ol_{Dia}, and some of the results are missing due to extremely low levels of Al and Cr. (**b**) includes the average *T* values (orange dots) of the different thermometers, and the error bars display the variance size corresponding to each dot.

Table 3. Correlation matrix of temperature values calculated using models three thermometers and their averages.

	T [Al-Ol, dH10-Dia]	T [Al-Ol, BW17]	T [Cr-Ol, dH10]	Average
T [Al-Ol, dH10-Dia]	1.00	1.00	0.99	1.00
T [Al-Ol, BW17]	1.00	1.00	0.95	0.99
T [Cr-Ol, dH10]	0.99	0.95	1.00	0.98
Average	1.00	0.99	0.98	1.00

The "Average" represents the average *T* value of the three thermometers on each Ol_{Dia}.

Important progress has been made on thermometers for different inclusions in diamonds in the Liaoning area. Previous research in the field has revealed a temperature range of 970–1330 °C [3,5,41–43], which is consistent with our T(average) range of 1080–1380 °C. These studies have mainly relied on the equilibrium temperature between the different mineral inclusions, such as those of Ca, Mg and Fe between garnet and omphacite [41] and the Mg/Fe partition geothermometer of olivine–garnet [42]. This research provides an important basis for understanding the thermal dynamics of diamond formation. The rare observation of these coexisting minerals has limited the practical application of such thermometers, so research on thermometers made of a single mineral in diamonds, such as garnet [3,43], Zn-in-chromite [43] and clinopyroxene thermometers [5] has introduced a new perspective to this field. However, these minerals are less commonly observed within diamonds in practical research. Given the considerable abundance of olivine inclusions in diamonds and the increasing amount of research on the behaviors of trace elements in them, we have reason to believe that the application of such thermometers to study how olivines constrain diamond formation is likely to significantly increase in the future. In other reports concerning Liaoning diamonds, records of olivine-related thermometers are still lacking. Therefore, this discovery not only provides an important reference for future research in related fields, but also enhances our understanding of the source conditions of olivine inclusions. Note that the widely adopted thermometers made of olivines are usually limited to garnet peridotitic olivines; however, the selection of a proper composition of Ol_{Dia}-related thermometers is very important, and we must consider a combination of different thermometers.

3. *P-T* constraints of Liaoning diamonds

According to T [Al-Ol, BW17] based on three Ol_{Dia} from Liaoning, a T^{LA} range of 1148–1196 °C was obtained. Combined with their pressure estimation [39], a projection of mantle *P-T* conditions predating their host diamond's formation was created (see Figure 7 with red dots). The result shows that the investigated samples follow a ~40 mW/m^2 conductive model geotherm.

In addition, a temperature estimation of 35 Ol_{Dia} based on data from previous studies yielded a *T*(average) range of 1114–1378 °C. The rough pressure could be derived via projections on to the geotherm, according to [19]. Further iterative calculation in combination with the simplified linear geotherm equation [38] and the equation (3) yielded new *P-T* values, which were then projected onto geotherms (see Figure 7, grey dots). Among the yielded 35 *P-T* values, many overlapped at T = 1128 °C, P = 50.7 kbar; T = 1244 °C, P = 48.5 kbar; T = 1366 °C, P = 55.7 kbar and T = 1411 °C, P = 57.9 kbar, resulting in only six distinct points visible on the plot. Among the 35 results, 31 fell within the geotherm range of 39–42 mW/m^2, while four reached the mantle adiabat. Notably, the high TiO_2 (>0.10 wt.%) revealed that the enrichment process occurred at a temperature greater than 1360–1400 °C, and pressure at 55–58 kbar (corresponding to a depth of around 161–178 km). Given potential inaccuracies produced through *T* estimation based on the EPMA data, the actual results may vary slightly. The results suggest Ti-rich metasomatic enrichments at the base of the lithospheric mantle beneath the NCC, which may have created favorable conditions for diamond formation. Such metasomatic processes have also been demonstrated according to clinopyroxene and garnet inclusions in Liaoning diamonds [5,44].

Our results are in alignment with previous reports on the combined *P* and *T* constraints of inclusions in Liaoning diamonds. A single clinopyroxene thermobarometer indicated a source environment with P = 53–61 kbar, T = 1080–1176 °C in the same locality, corresponding to a ~40 mW/m^2 geotherm [45]. A similar range of 35–40 mW/m^2 geotherm has been obtained using a combination of thermometers and barometers [33,43,46].

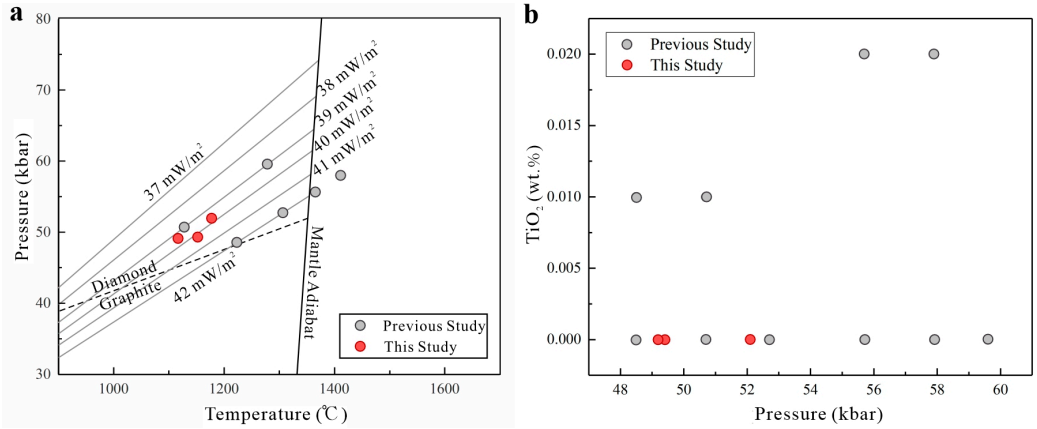

Figure 7. (**a**) *P-T* estimation of Liaoning diamonds based on olivine inclusion, with geotherms mantle adiabat from [38]. The diamond/graphite transition [47] is shown for reference. Data from a previous study were obtained via iterative calculation (see text). The results show overlap, with 19 points at T = 1128 °C, P = 50.7 kbar; 10 points at T = 1244 °C, P = 48.5 kbar; 1 point at T = 1279 °C, P = 59.6 kbar; 1 point at T = 1307 °C, P = 52.7 kbar; 2 points at T = 1366 °C, P = 55.7 kbar; and 2 points at T = 1411 °C, P = 57.9 kbar. The Ol_{Dia} from Liaoning mainly fall along geotherms at 39–41 mW/m^2 and 42 mW/m^2, while four results fall within the mantle adiabatic region. (**b**) TiO_2 content (wt.%) versus pressure of Ol_{Dia}. TiO_2 (≥0.10 wt.%) enrichment corresponds to a variety range of pressure.

5. Conclusions

The geochemistry of Ol_{Dia} provides evidence for the heterogeneity of the lithospheric mantle beneath the NCC. The high Mg# number, together with the high Cr# number and low TiO_2 content of the most Ol_{Dia}, suggests the depletion of the lithospheric mantle where

Liaoning diamonds formed. However, 34% of the Liaoning Ol_{Dia} showed a relatively rich TiO_2 content and high Cr# number, suggesting a re-fertilization process in the NCC. Therefore, Ti-rich metasomatism may take place at the base of the lithospheric mantle (at around 161–178 km).

In addition, the application of olivine thermometers (T [Al-Ol, dH10-Dia], T [Cr-Ol, dH10], T [Al-Ol, BW17]) is important for understanding the formation mechanism of Liaoning diamonds. T^{LA} provided the highest accuracy for temperature estimates, and among different thermometers, the use of T [Al-Ol, BW17] is recommended. A comparison of T^{EPMA} and T^{LA} suggested lower deviation of the T estimates with T [Cr-Ol, dH10] and on the T(average). Therefore, averaging the results from multiple thermometers is recommended to minimize inaccuracies in EPMA measurements.

A total of 90 T values were obtained through calculation using EPMA data for 35 Ol_{Dia}, with the average falling within the range of 1114–1378 °C. By comparing the T values calculated using the three thermometers and their correlation with each other and their averages, we confirmed that T [Al-Ol, dH10-Dia], T [Cr-Ol, dH10] and T [Al-Ol, BW17] were consistent. These findings provide insights for optimizing model selection and improving the accuracy of olivine sample temperature calculations.

Together with the T^{LA} for the three investigated Ol_{Dia}, we presented diamond source conditions with T ranging from 1080 to 1380 °C, aligning with previous reports on Liaoning diamonds based on evidence from other thermobarometers. Projections onto geotherms for these Ol_{Dia} yielded the conductive model geotherm of 39–42 mW/m^2 in the lithospheric mantle beneath the NCC.

Supplementary Materials: The following supporting information can be downloaded at: https://www.mdpi.com/article/10.3390/min14090850/s1, Table S1: Compositional data of 62 olivine inclusions in diamonds from Liaoning; Table S2. Temperature estimation using three thermometers based on EPMA data for 35 samples.

Author Contributions: Conceptualization, L.Q. and G.S.; methodology, L.Q.; validation, L.Q., G.S., X.Z. and Z.C.; formal analysis, L.Q.; investigation, L.Q.; resources, X.Z.; data curation, L.Q.; writing—original draft preparation, L.Q.; writing—review and editing, G.S. and Z.C.; visualization, L.Q.; supervision, G.S.; project administration, G.S.; funding acquisition, G.S. All authors have read and agreed to the published version of the manuscript.

Funding: This research was funded by National Natural Science Foundation of China (Grant No. 42273044).

Data Availability Statement: All data generated or used during the study appear in the submitted article.

Acknowledgments: Photos of diamonds are taken at the Experimental Teaching Center of Gemology, China University of Geosciences (Beijing).

Conflicts of Interest: The authors declare no conflicts of interest.

References

1. Gordeychik, B.; Churikova, T.; Shea, T.; Kronz, A.; Simakin, A.; Wörner, G. Fo and Ni Relations in Olivine Differentiate between Crystallization and Diffusion Trends. *J. Petrol.* **2020**, *61*, 1–23. [CrossRef]
2. Zhu, R.-Z.; Ni, P.; Wang, G.-G.; Ding, J.-Y.; Kang, N. Temperature and oxygen state of kimberlite magma from the North China Craton and their implication for diamond survival. *Miner. Depos.* **2022**, *57*, 301–318. [CrossRef]
3. Liu, L.; Wu, D.; Han, S.; Wan, F.; Lin, S.; Yang, X. Study of kimberlite type diamond deposit and its metallogenic model—An example of the primary diamond deposit in the Wafangdian area of Liaoning province (In Chinese with English Abstract). *Acta Geol. Sin.* **2020**, *94*, 2650–2665.
4. Zhao, D. Electron Probe Microanalysis and Microscopy of Polishing-Exposed Solid-Phase Mineral Inclusions in Fuxian Kimberlite Diamonds. *Minerals* **2022**, *12*, 844. [CrossRef]
5. Wang, W.; Gasparik, T. Metasomatic clinopyroxene inclusions in diamonds from the Liaoning Province, China. *Geochim. Cosmochim. Acta* **2001**, *65*, 611–620. [CrossRef]
6. Qi, L.; Tang, Z.; Lu, X.; He, M.; Zhang, F.; Miao, Q. Typomorphic peculiarities and significance of mineral inclusions in diamond in Liaoning province, China. *J. Gems Gemmol.* **1999**, *1*, 27–34, (In Chinese with English Abstract)

7. Wang, W. Formation of diamond with mineral inclusions of "mixed" eclogite and peridotite paragenesis. *Earth Planet. Sci. Lett.* **1998**, *160*, 831–843. [CrossRef]
8. Wang, Z.; Guo, G. Characteristics of inclusions from diamond in No.50 pipe at Wafangdian, south Liaoning. *Liaoning Geol.* **1994**, *11*, 263–274, (In Chinese with English abstract)
9. Stachel, T.; Harris, J.W. The origin of cratonic diamonds—Constraints from mineral inclusions. *Ore Geol. Rev.* **2008**, *34*, 5–32. [CrossRef]
10. De Hoog, J.C.M.; Gall, L.; Cornell, D.H. Trace-element geochemistry of mantle olivine and application to mantle petrogenesis and geothermobarometry. *Chem. Geol.* **2010**, *270*, 196–215. [CrossRef]
11. Meyer, H.O.A. *Inclusions in Diamond*; Wiley: Chichester, UK, 1987.
12. Stachel, T.; Aulbach, S.; Harris, J.W. Mineral Inclusions in Lithospheric Diamonds. *Rev. Mineral. Geochem.* **2022**, *88*, 307–391. [CrossRef]
13. De Hoog, J.C.M.; Stachel, T.; Harris, J.W. Trace-element geochemistry of diamond-hosted olivine inclusions from the Akwatia Mine, West African Craton: Implications for diamond paragenesis and geothermobarometry. *Contrib. Mineral. Petrol.* **2019**, *174*, 28. [CrossRef]
14. Zhang, L.; Li, N.; Dejan, P. The research status of olivine trace elements in-situ analysis and perspectives of its application. *Acta Petrol. Sin.* **2016**, *32*, 1877–1890, (In Chinese with English Abstract)
15. Nimis, P. Pressure and Temperature Data for Diamonds. *Rev. Mineral. Geochem.* **2022**, *88*, 533–565. [CrossRef]
16. Stosch, H.-G. Sc, Cr, Co and Ni partitioning between minerals from spinel peridotite xenoliths. *Contrib. Mineral. Petrol.* **1981**, *78*, 166–174. [CrossRef]
17. O'Reilly, S.Y.; Griffin, W.L.; Ryan, C.G. Minor elements in olivine from spinel lherzolite xenoliths; implications for thermobarometry. *Mineral. Mag.* **1997**, *61*, 257–269. [CrossRef]
18. Witt-Eickschen, G.; O'Neill, H.S.C. The effect of temperature on the equilibrium distribution of trace elements between clinopyroxene, orthopyroxene, olivine and spinel in upper mantle peridotite. *Chem. Geol.* **2005**, *221*, 65–101. [CrossRef]
19. Bussweiler, Y.; Brey, G.P.; Pearson, D.G.; Stachel, T.; Stern, R.A.; Hardman, M.F.; Kjarsgaard, B.A.; Jackson, S.E. The aluminum-in-olivine thermometer for mantle peridotites—Experimental versus empirical calibration and potential applications. *Lithos* **2017**, *272–273*, 301–314. [CrossRef]
20. Korolev, N.M.; Kopylova, M.; Bussweiler, Y.; Pearson, D.G.; Gurney, J.; Davidson, J. The uniquely high-temperature character of Cullinan diamonds: A signature of the Bushveld mantle plume? *Lithos* **2018**, *304–307*, 362–373. [CrossRef]
21. Nimis, P.; Alvaro, M.; Nestola, F.; Angel, R.J.; Marquardt, K.; Rustioni, G.; Harris, J.W.; Marone, F. First evidence of hydrous silicic fluid films around solid inclusions in gem-quality diamonds. *Lithos* **2016**, *260*, 384–389. [CrossRef]
22. Hunt, J.D.; Kavner, A.; Schauble, E.A.; Snyder, D.; Manning, C.E. Polymerization of aqueous silica in H_2O–K_2O solutions at 25–200 °C and 1bar to 20kbar. *Chem. Geol.* **2011**, *283*, 161–170. [CrossRef]
23. Zotov, N.; Keppler, H. Silica speciation in aqueous fluids at high pressures and high temperatures. *Chem. Geol.* **2002**, *184*, 71–82. [CrossRef]
24. Gurney, J.J.; Helmstaedt, H.; Moore, R.O. A review of the use and application of mantle mineral geochemistry in diamond exploration. *Pure Appl. Chem.* **1993**, *65*, 2423–2442. [CrossRef]
25. Zheng, J.P.; Lu, F.X. Mantle xenoliths from kimberlites, Shandong and Liaoning: Paleozoic mantle character and its heterogeneity. *Acta Pet. Sin.* **1999**, *15*, 65–74, (In Chinese with English Abstract)
26. Duan, X.; Shen, H.; Li, N.; Xiao, W.; Sui, Q.; He, H.; Feng, P.; Tang, Z. Transformation of the Sub-Continental Lithospheric Mantle Beneath the North China Craton (NCC): Constraints from the Geochemical Characteristics of Olivine Websterite Xenoliths and Their Minerals in the Cenozoic Basalts from Hannuoba. *Minerals* **2022**, *12*, 401. [CrossRef]
27. Xu, W.; Zhou, Q.; Pei, F.; Yang, D.; Gao, S.; Li, Q.; Yang, Y. Destruction of the North China Craton: Delamination or thermal/chemical erosion? Mineral chemistry and oxygen isotope insights from websterite xenoliths. *Gondwana Res.* **2013**, *23*, 119–129. [CrossRef]
28. Tang, Y.; Ying, J.; Zhao, Y.; Xu, X. Nature and secular evolution of the lithospheric mantle beneath the North China Craton. *Sci. China Earth Sci.* **2021**, *64*, 1492–1503. [CrossRef]
29. Zhu, R.; Xu, Y.; Zhu, G.; Zhang, H.; Xia, Q.; Zheng, T. Destruction of the North China Craton. *Sci. China Earth Sci.* **2012**, *55*, 1565–1587. [CrossRef]
30. Zhu, R.; Xu, Y. The subduction of the west Pacific plate and the destruction of the North China Craton. *Sci. China Earth Sci.* **2019**, *62*, 1340–1350. [CrossRef]
31. Cartigny, P.; Palot, M.; Thomassot, E.; Harris, J.W. Diamond Formation: A Stable Isotope Perspective. *Annu. Rev. Earth Planet. Sci.* **2014**, *42*, 699–732. [CrossRef]
32. Bureau, H.; Remusat, L.; Esteve, I.; Pinti, D.L.; Cartigny, P. The growth of lithospheric diamonds. *Sci. Adv.* **2018**, *4*, eaat1602. [CrossRef]
33. Ashchepkov, I.; Logvinova, A.; Spetsius, Z.; Downes, H. Thermobarometry of diamond inclusions: Mantle structure and evolution beneath Archean cratons and mobile belts worldwide. *Geosyst. Geoenviron.* **2023**, *2*, 1–22. [CrossRef]
34. Bureau, H.; Frost, D.J.; Bolfan-Casanova, N.; Leroy, C.; Esteve, I.; Cordier, P. Diamond growth in mantle fluids. *Lithos* **2016**, *265*, 4–15. [CrossRef]

35. Jean, M.M.; Taylor, L.A.; Howarth, G.H.; Peslier, A.H.; Fedele, L.; Bodnar, R.J.; Guan, Y.; Doucet, L.S.; Ionov, D.A.; Logvinova, A.M.; et al. Olivine inclusions in Siberian diamonds and mantle xenoliths: Contrasting water and trace-element contents. *Lithos* **2016**, *265*, 31–41. [CrossRef]
36. Brey, G.P.; Kohler, T. Geothermobarometry in Four-phase Lherzolites II. New Thermobarometers, and Practical Assessment of Existing Thermobarometers. *J. Petrol.* **1990**, *31*, 1353–1378. [CrossRef]
37. Li, J.; O'Neil, H.S.C.; Seifert, F. Subsolidus Phase Relations in the System MgO—SiO_2—Gr—O in Equilibrium with Metallic Cr, and their Significance for the Petrochemistry of Chromium. *J. Petrol.* **1995**, *36*, 107–132. [CrossRef]
38. Hasterok, D.; Chapman, D.S. Heat production and geotherms for the continental lithosphere. *Earth Planet. Sci. Lett.* **2011**, *307*, 59–70. [CrossRef]
39. Qin, L.; Shi, G.; Zhao, X. The source pressure of diamond from North China Craton-Constraints from the olivine inclusions. *Geol. Rev.* **2023**, *69*, 93–94. (In Chinese)
40. Stachel, T. *.PTEXL—Geothermobarometry of Mantle Rocks*, V1 ed.; Borealis: Vienna, Austria, 2022. [CrossRef]
41. Miao, Q. Paragenetic mineral inclusions of ultramafic rock and eclogite in the same diamond. *Liaoning Geol.* **1996**, *13*, 39–46, (In Chinese with English Abstract).
42. Wang, W.; Takahashi, E.; Sueno, S. Geochemical properties of lithospheric mantle beneath the Sino-Korea craton; evidence from garnet xenocrysts and diamond inclusions. *Phys. Earth Planet. Inter.* **1998**, *107*, 249–260. [CrossRef]
43. Zhang, A.; Griffin, W.L.; Ryan, C.G.; Andrew, A. Conditions of diamond formation beneath the Sino-Korean craton: Paragenesis, temperatures and the isotopic composition of carbon. In Proceedings of the International Kimberlite Conference: Extended Abstracts, Cape Town, South Africa, 17 April 1998; pp. 992–994.
44. Wang, W.; Sueno, S.; Takahashi, E.; Yurimoto, H.; Gasparik, T. Enrichment processes at the base of the Archean lithospheric mantle: Observations from trace element characteristics of pyropic garnet inclusions in diamonds. *Contrib. Mineral. Petrol.* **2000**, *139*, 720–733. [CrossRef]
45. Yin, L.; Zhang, R.; Zheng, J. Mineral Chemistry Characters of Diamond Inclusions and the Nature of the Lithospheric Mantle beneath the Eastern North China Craton. *Geol. Sci. Technol. Inf.* **2008**, *27*, 21–28, (In Chinese with English Abstract)
46. Wang, Y.J.; Nestola, F.; Li, H.K.; Hou, Z.Q.; Pamato, M.G.; Novella, D.; Lorenzetti, A.; Antignani, P.A.; Cornale, P.; Nava, J.; et al. In situ single-crystal X-ray diffraction of olivine inclusion in diamondfrom Shandong, China: Implications for the depth of diamond formation. *Eur. J. Mineral.* **2023**, *35*, 361–372. [CrossRef]
47. Day, H.W. A revised diamond-graphite transition curve. *Am. Mineral.* **2012**, *97*, 52–62. [CrossRef]